Journal of Materials Chemistry A

Accepted Manuscript

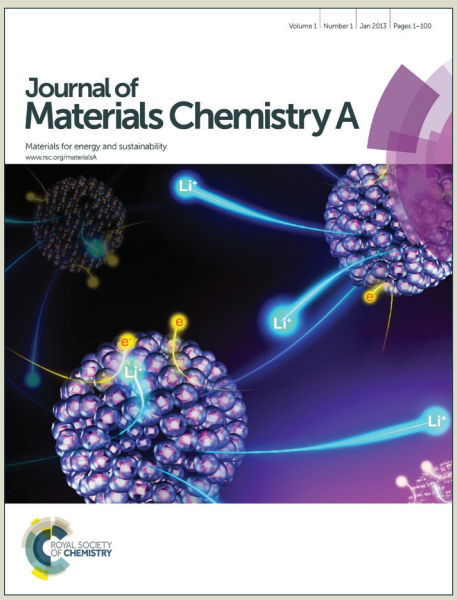

ROYAL SOCIETY OF CHEMISTRY

www.rsc.org/materialsA

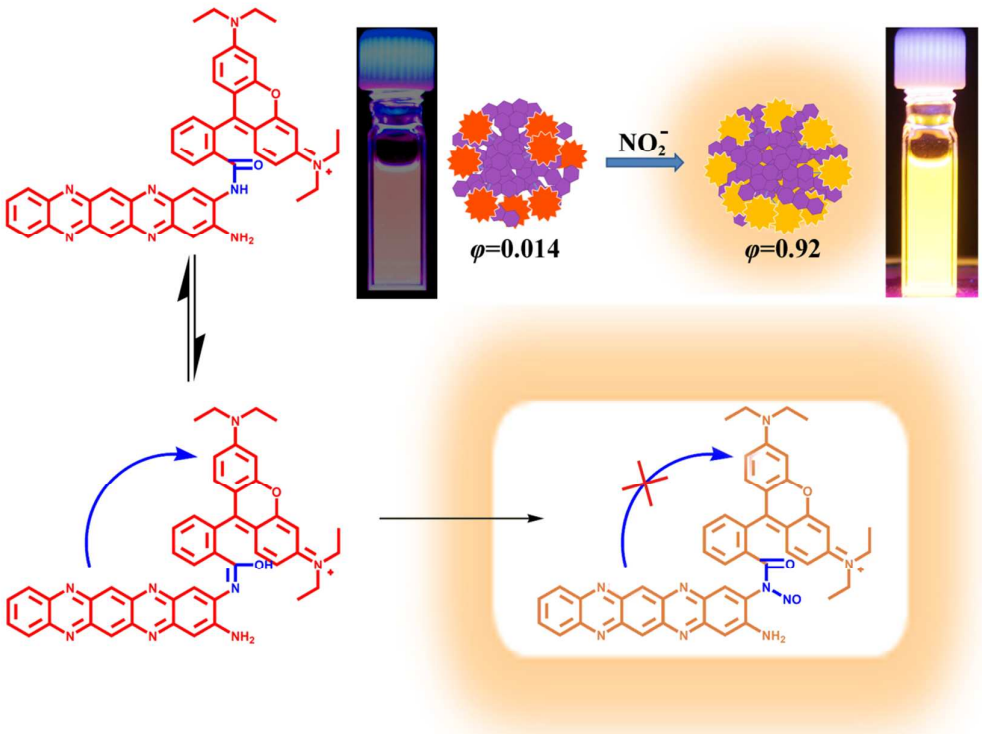

Cite this: DOI: 10.1039/c0xx00000x

www.rsc.org/xxxxxx

ARTICLE TYPE

Photoinduced electron transfer of poly(o-phenylenediamine)-Rhodamine B copolymer dots: application in ultrasensitive detection of nitrite *in vivo*

Fang Liao,[a 1 *] Xun Song,[a 1] Siwei Yang,[a b *] Chenyao Hu,[c] Lin He,[a] Shuai Yan,[a] and Guqiao Ding, [b *]

Received (in XXX, XXX) Xth XXXXXXXXX 20XX, Accepted Xth XXXXXXXXX 20XX

DOI: 10.1039/b000000x

We demonstrate a new semiconducting polymer dot: the poly(o-phenylenediamine)-Rhodamine B copolymer dots (Pp-RhB dots), which emits in the red wavelength range. The Pp-RhB dots can be used as a ultrasensitive fluorescence probe for NO_2^- *in vivo* and show high selectivity and ultrasensitivity (detection limit: 2.0×10^{-11} M) for NO_2^-. The fluorescence of Pp-RhB dots is decreased ($\varphi = 0.014$) as a result of fast photoinduced electron transfer (PET) between the modulator (poly(o-phenylenediamine)) and the transducer (RhB), but the N-NO_2 bonding mode prevents PET, causing the fluorescence emission to be enhanced ($\varphi = 0.92$). This probe effectively avoids the influence of auto-fluorescence in biological systems and gave positive results when tested in both aqueous solution and living cells.

Introduction

As a new fluorescent material, semiconducting polymer dots (Pdots) have been the subject of increasing research attention due to their large absorption cross-sections, high quantum yields, excellent photostability and rapid emission rates. [1-8] Compared with semiconductor quantum dots and graphene quantum dots, Pdots are easily prepared, cheap, and of low bio-toxicity. [9-16] With diversified, and definite molecular, structures, Pdots are easily modified and may have peculiar molecular recognition abilities. [17-19] Moreover, the optical properties of Pdots can be easily modulated and obtain red (620-700 nm) or near-IR (650-900 nm) emitting fluorescent materials which allows deep penetration into tissues and efficaciously avoids the influence of bioautofluorescence. Chiu *et al.* reported various Pdots with controllable PL properties and applied them to biological imaging and bioanalytical applications. [1-6] However, it is still imperative to develop new Pdots with various properties for biological imaging and bioanalytical applications.

On the other hand, nitrite (NO_2^-) which is a mesostate in the nitrogen cycle, resulting from oxidation of ammonia or from reduction of nitrate, can enhance the possibility of cancer and deformities. [20-22] Moreover, peroxynitrite can be obtained in the metabolism of NO_2^- which is a potent cytotoxic agent produced by rapid combination of NO and O_2^-·*in vivo*: it can nitrate tyrosine residues of insulin. [21] NO_2^- was also used in the preservation of meat and fish products, can interact with amines, and form carcinogenic compounds such as nitrosamines. Thus, the quantitative determination of NO_2^- *in vivo*, in water, food, and agricultural products is important. [23] The World Health Organisation (WHO) recommends a maximum limit of nitrite ions in drinking water of 6.5×10^{-5} M. [24] Nowadays, most rapid detection methods for NO_2^- are based on organic dyes. [21-23] However, the design, synthesis, and preparation of most organic dyes are complex. In addition, the low stability, weak anti-jamming ability, and potential cytotoxicity of these dyes to organisms restrict their widespread application.

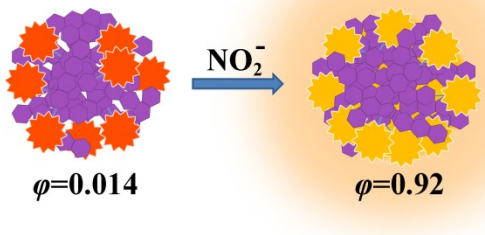

Scheme 1. A schematic diagram of the working mechanism of Pp-RhB dots.

Here, we demonstrate a new Pdot: poly(o-phenylenediamine)-Rhodamine B copolymer dots (Pp-RhB dots), which emits in the red wavelength range. The fluorescence of Pp-RhB dots is decreased ($\varphi = 0.014$) as a result of fast photoinduced electron transfer (PET) between the modulator (poly(o-phenylenediamine)) and the transducer (RhB). However, when NO_2^- was added the N-NO_2 bonding mode prevented the PET, causing the fluorescence emission to be enhanced ($\varphi = 0.92$). As the concentrations of NO_2^- were increased from 5×10^{-10} M to 2×10^{-9} M, the photoluminescence (PL) peak at 681 nm was steadily decreased, which was accompanied by a simultaneous increase in the intensity of the PL peak at 599 nm. This Pp-RhB dots can be used as an ultrasensitive fluorescence probe for NO_2^- *in vivo* and showed high selectivity and ultrasensitivity (detection limit: 2.0×10^{-11} M) for NO_2^- in both aqueous solution and living cells.

Materials and methods

Materials

Rhodamine B (RhB, 99.0%), o-phenylenediamine (oPD, 98.0%), $(NH_4)_2S_2O_8$ (APS, 99.5%), NaCl (99.5%), KCl (99.5%), $LiNO_3$ (99.5%), $MgCl_2$ (99.5%), $ZnCl_2$ (99.5%), $NiCl_2$ (99.5%), $CdCl_2$ (99.5%), $PbCl_2$ (99.5%), $FeCl_2$ (99.0%), $FeCl_3$ (99.5%), $AlCl_3$ (99.0%), KBr (99.5%), Na_2SO_4 (99.5%), and K_2HPO_4 (99.5%) were purchased from Aladdin (Shanghai, China) and used as received without further purification. The water used throughout all experiments was purified through a Millipore system.

Synthesis of Pp-RhB dots

Typically, 2.0 mL, 20 mM oPD aqueous solution was added into a mixture of 0.3 mL, 40 mM RhB aqueous solution and 2.0 mL, 20 mM APS aqueous solution. Then, the mixture was transferred into a 15 mL Teflon®-lined autoclave and heated to 260 °C and maintained at that temperature for 12 h before being allowed to cool naturally to room temperature. The product was filtered through a 0.02 μm micro-porous membrane and a yellow transparent filter solution was obtained. The black precipitates were discarded. The resulting orange filtrate was dialysed in a 500 Da dialysis bag against deionised water for a week to remove excess salt. The yield was approximately 25%.

Characterisation methods

Transmission electron microscopy (TEM) measurements were carried out on a Hitachi H-8100 EM (Hitachi, Tokyo, Japan) with an accelerating voltage of 200 kV. X-ray photoelectron spectra (XPS) were recorded on a PHI Quantera II system (Ulvac-PHI, Inc, Japan). Fluorescent emission and excitation spectra were recorded on a PerkinElmer LS55 luminescence spectrometer (PerkinElmer Instruments, U.K.) at room temperature (25 °C) in aqueous solution. The stability of these products was determined by contrasting the fluorescent emission intensity of products in aqueous solution under different conservation times at room temperature (25 °C). Quantum yield (Φ_f) was measured according to an established procedure (Lakowicz, J. R. Principles of Fluorescence Spectroscopy, 2nd Ed., 1999, Kluwer Academic/Plenum Publishers, New York). The UV-vis spectra were obtained on a UV5800 Spectrophotometer. Rhodamine 6G solution (quantum yield 0.98 in EtOH) was chosen as a standard. Absolute values were calculated using the standard reference sample that had a fixed, known, fluorescence quantum yield value. To minimise re-absorption effects, absorbencies in the 10 mm fluorescence cuvette were kept under 0.1 at the excitation wavelength. Time-resolved fluorescence behaviour was measured by time-correlated single-photon counting (TCSPC) technique (HydraHarp 400, PicoQuant). The samples were excited by frequency-doubled titanium: sapphire oscillator laser with an approximate pulse duration of 150 fs, and a repetition frequency of 80 MHz (Chameleon, Coherent). Fluorescence emission was sent to a spectrometer (iHR550, Horiba Jobin Yvon) with 300/mm grating and then detected by a photomultiplier tube.

Cellular test

The HeLa cell line was obtained from the Cell Bank of The Chinese Academy of Science and cultured in the standard medium at 37 °C in 5% CO_2. Cells were seeded in a 96-well plate for 24 h before Pp-RhB dots treatment. Serial dilutions of Pp-RhB dots with known concentrations were added to the cells. After 24 h incubation, the relative viabilities of cell samples were determined by colorimetric 3-(4, 5-dimethylthiazol-2-yl)-2, 5-diphenyl tetrazolium bromide (MTT) assays performed to assess the metabolic activity of cells treated as described above. Cells were lysed with acidulated sodium dodecyl sulphate (SDS). Absorbance was measured at 570 nm using a micro-plate reader (Bio-Rad 680, U.S.A.). All measurements were done in triplicate, and at least three independent experiments were carried out.

Results and discussion

The low magnification TEM image and corresponding size distribution histogram of Pp-RhB dots thus formed are shown in Fig. 1a. Homogeneous dots with a lateral size distribution of 1 to 4 nm and an average diameter of 1.86 nm were found. Fig. 1b and c show a representative high-resolution TEM image and the corresponding fast Fourier transform (FFT) result of an individual Pp-RhB dot. There was no crystalline structure in these obtained Pp-RhB dots which indicated an amorphous structure to these Pp-RhB dots. AFM observations (Fig. 1d and e) show highly dispersed Pp-RhB dots on the silicon substrate with a typical topographic height of 1 to 1.5 nm.

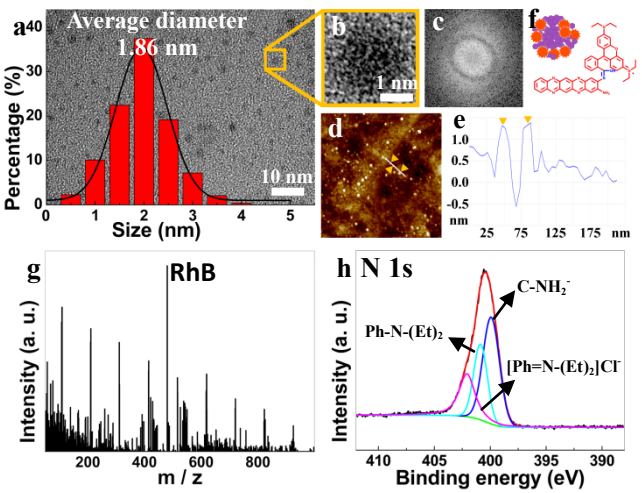

Fig. 1 (a) TEM image and corresponding size distribution histogram of Pp-RhB dots, (b) HRTEM image of a single Pp-RhB dot particle, (c) FFT of a single dot in (a), (d) AFM topography image of Pp-RhB dots on a mica substrate in tapping mode (Bruker Dimension Icon AFM microscope), (e) height profile analysis along the line shown in the image. (f) A schematic of the structure of Pp-RhB dots. (g) MALDI-TOF-MASS spectrum for hydrolysates of Pp-RhB dots after refluxing in 0.1 M HCl for 12 h. (h) N1s spectra of Pp-RhB dots.

The MALDI-TOF-MASS spectra, XPS spectra, and FT-IR spectra were analysed to verify the structure and formation of Pp-RhB dots. As shown in Fig. 1g, the MALDI-TOF-MASS spectra for hydrolysates of Pp-RhB dots after refluxing in 0.1 M HCl for 12 h indicates 10 peaks which can be attributed to the RhB and oligomers of PoPD. The peak located at m/z = 508.05 can be attributed to the protonated RhB. The peaks located at m/z = 109.20 can be attributed to the protonated monomer (oPD). Moreover, the peaks located at m/z = 212.04, 311.69, 415.92, 517.57, 620.01, 721.85, 824.29, and 926.14 can be attributed to

the protonated dimer, trimer, tetramer, and oligomers of oPD, respectively. [4b, 8b, 25-29]

The XPS survey spectrum (Fig. S1) for Pp-RhB dots shows a predominant narrow graphitic C 1s peak at *c*. 284 eV, along with a N 1s peak at *c*. 399 eV, and an O 1s peak at *ca*. 532 eV. [30] The elemental composition of Pp-RhB dots is shown in Table S1. The well-fitted C1s XPS spectrum of Pp-RhB dots is shown in Fig. S2. The C1s XPS spectrum can be divided into four peaks, which correspond to the signals of C-C (284.6 eV), C-O-C (286.0 eV), C-N (285.2 eV), and C=O (282.9 eV). [31] Two peaks can be found in the O1s XPS (Fig. S3) spectrum which indicated the existence of C-O-C (533.4 eV) and C=O (532.0 eV) bonding models in Pp-RhB dots. The N1s XPS spectrum (Fig. 1h) indicated the existence of $[Ph{=}N\text{-}(Et)_2]Cl^-$ (402.1 eV), Ph-N-$(Et)_2$ (400.9 eV), and C-NH_2 (399.9 eV) bonding models in Pp-RhB dots. [32] Furthermore, the peak located at 1668 cm^{-1} in FT-IR spectra (Fig. S4) proved the existence of an amide bond in the Pp-RhB dots. [31c, d]

UV-vis absorption and PL spectroscopy were carried out to investigate the spectral properties of Pp-RhB dots. Fig. 2a shows the UV–vis absorption spectrum of RhB and Pp-RhB dots. The bonding between RhB and PoPD caused a bathochromic shift of 32 nm relative to RhB while a broad peak at *ca*. 610 to 780 nm appeared. The bathochromic shift in the absorption spectrum was due to the larger conjugated structure in the main chain of the Pp-RhB dots.

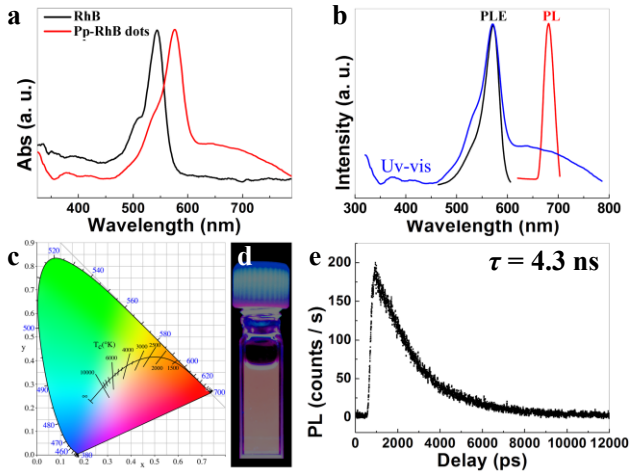

Fig. 2 (a) Normalised UV–vis absorption spectrum of RhB (black curve) and Pp-RhB dots (red curve). (b) Normalised PL (red curve λ_{ex} = 572 nm) and PLE (black curve λ_{em} = 681 nm) and UV–vis absorption (blue curve) spectra of Pp-RhB dots in aqueous solution. (c) The CIE chromaticity coordinates for Pp-RhB dots in aqueous solution. (d) Digital image of Pp-RhB dots in aqueous solution under UV-light (centre wavelength: 365 nm). (e) PL decay curves of Pp-RhB dots measured at room temperature with λ_{em} = 681 nm.

The Pp-RhB dots exhibited maximum excitation (λ_{ex}) and emission (λ_{em}) wavelengths at 572 and 681 nm, respectively. The optimum excitation condition corresponded to the UV-vis peak at 570 nm. Further experiments explored the PL properties of as-synthesised Pp-RhB dots: a detailed PL study was carried out with different excitation wavelengths. Excitation wavelength dependency is a common phenomenon in graphene quantum dots and carbon dots which can be attributed to the diverse chromophores in these dots. However, for Pp-RhB dots, when λ_{ex} was increased from 500 to 600 nm, the emission peak did not shift by any more than a maximum red shift of 5 nm (Fig. S5). This showed that the Pp-RhB dots have unified chromophores. The Stokes shift ($\Delta\nu_{St}$) of the Pp-RhB dots was 0.35 eV. The half-maximum (FWHM) of the PL spectra of Pp-RhB dots is 0.05 eV (20 nm). This indicated that the Pp-RhB dots had a weak self-absorption effect and low energy loss. [27] Moreover, the narrowing of FWHM (which was much small than that in graphene quantum dots, carbon dots, or polymer dots) also indicated the presence of unified chromophores in Pp-RhB dots.

The Commission Internationale de l'Eclairage (CIE) chromaticity coordinates for Pp-RhB dots are shown in Fig. 2c. The CIE chromaticity coordinates of the Pp-RhB dots were (0.72, 0.28). The Pp-RhB dots in aqueous solution excited by a 365 nm lamp (6 W) emitted a weak red luminescence (Fig. 2c) with a low quantum yield (0.014). The fluorescence of Pp-RhB dots was weakened as a result of the fast PET process between the modulator (PoPD) and the transducer (RhB). The PL decay of Pp-RhB dots was measured by a time-correlated single photon counting technique, and fitted well with a bi-exponential decay as shown in Fig. 2e. The lifetime (τ) was dominated by a long decay component of 4.4 ns (96%) plus a small contribution from the short decay of 2.1 ns (4%): the weighted-average lifetime was approximately 4.3 ns. The fluorescence radiative rate κ_r of Pp-RhB dots can be obtained by combining φ and τ as follows: $\kappa_r = \varphi/\tau$. The κ_r value for Pp-RhB dots was 3.25 × 10^6 s^{-1}. The low radiative rate implied a significant quenching of the PET process between PoPD and RhB. [33-34]

The stability of Pp-RhB dots is important for practical applications. Here, the photostability of Pp-RhB dots was also considered. The Pp-RhB dots showed excellent stability after continuous excitation under visible light for more than 90 days (see red curve in Fig. 2a), or ultraviolet radiation (150 W Xe lamp with a centre wavelength of 320 nm, 48 h, see black curve in Fig. 2a). By contrast, the RhB showed weak stability under ultraviolet radiation. This indicated that the Pp-RhB dots had much better stability than fluorescent dyes. The PL intensity of Se-GQDs was also stable when the pH value was changed from 4 to 10 (Fig. S6). This meant that these polymer dots were stable and could be used in most biological environments.

Table 1. Comparison of different NO_2^- detection methods.

Detection method	Detection limit	Ref.
Spectrophotofluorimetry	1.84 × 10^{-6} g	36
Fluorescence quenching (CDs)	5.3 × 10^{-8} M	37
Negative chemical ionisation	3.3 × 10^{-9} M	38
HPLC	1 × 10^{-4} M	39
Electron transfer	6.2 × 10^{-8} M	40
Paper-based microfluidic	4.6 × 10^{-5} g	41
Solid-state microelectrode	3 × 10^{-5} M	42
Capillary electrochromatography	9 × 10^{-5} M	43
Raman spectroscopy	4.6 × 10^{-5} g	44
Lab.-on-chip measurement	9.2 × 10^{-7} g	45
Electrochemical sensor	6.624 × 10^{-6} M	46

Au nanoparticles	1.01×10^{-3} g	47
UV resonance Raman	$< 6.44 \times 10^{-4}$ g	48
Mediator-modified electrodes	4.6×10^{-5} g	49
Colorimetric probe	4.35×10^{-4} M	50

We further explored the feasibility of using these Pp-RhB dots for the detection of NO_2^-. As the concentration of NO_2^- was increased from 5×10^{-10} M to 2×10^{-9} M, the PL peak at 681 nm gradually decreased, while the PL peak at 599 nm increased (Fig. 3b, c). The CIE chromaticity coordinates of the Pp-RhB dots moved to (0.63, 0.37) and they emitted a strong orange luminescence (Fig. 3d) with a high quantum yield (0.92) when the concentration of NO_2^- was higher than 2×10^{-9} M. The lifetime (τ) was dominated by a long decay component of 4.0 ns (97%) plus a small contribution from the short decay of 2.2 ns (3%): the weighted-average lifetime was approximately 3.9 ns. The fluorescence radiative rate κ_r of Pp-RhB dots can be obtained by combining φ and τ as follows: $\kappa_r = \varphi/\tau$. The κ_r value of the Pp-RhB dots was 2.36×10^8 s^{-1}. The κ_r value was much higher than that without NO_2^- being present.

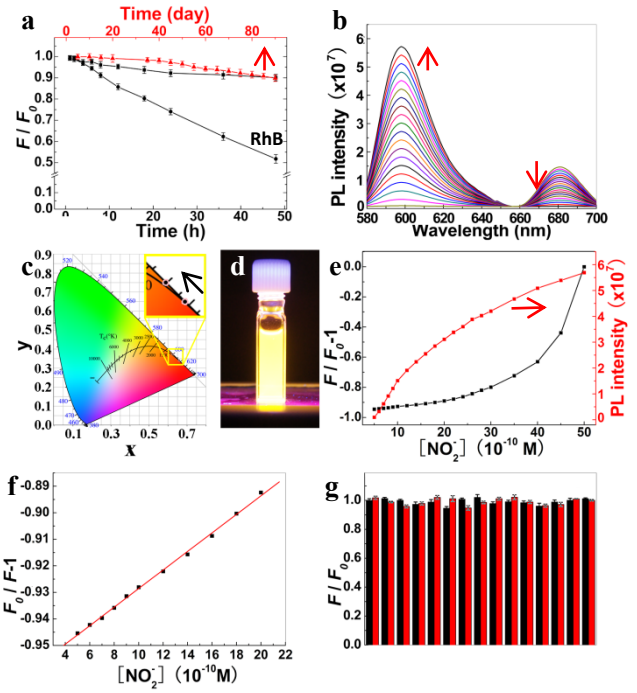

Fig. 3(a) Stability of Pp-RhB dots under visible light (red curve) at room temperature. Photo-stability (black curves) of Pp-RhB dots and RhB under UV light (150 W Xe lamp with a centre wavelength of 320 nm). F_0 and F are initial (t = 0), and specific time, PL intensities, respectively. (b) PL spectra of Pp-RhB dots with different concentrations of NO_2^- (5×10^{-10} M to 2×10^{-9} M) with an emission wavelength of 572 nm at 25 °C and pH = 7. The concentration of Pp-RhB dots was 1.0 mg mL^{-1}. (c) The CIE chromaticity coordinates for Pp-RhB dots in aqueous solution in the absence and presence of NO_2^-. (d) Digital image of Pp-RhB dots in aqueous solution in the presence of NO_2^- under UV-light (centre wavelength: 365 nm). (e) Black curve: the Stern-Volmer plot of the PL peak at 681 nm for different NO_2^- concentrations. Red curve: the intensity of the PL peak at 599 nm for different NO_2^- concentrations. (f) Linear fitting of the Stern-Volmer plot of the PL peak at 681 nm for different NO_2^- concentrations (5×10^{-10} M to 2×10^{-9} M). (g) The difference in PL intensity of Pp-RhB dots between the blank and solutions containing different metal ions with (red) and without (black) the presence of NO_2^- (F_0 and F are PL intensities in the absence and presence of these ions, respectively). The ions are: Na^+, K^+, Li^+, Mg^{2+}, Zn^{2+}, Ni^{2+}, Cd^{2+}, Pb^{2+}, Fe^{2+}, Fe^{3+}, Al^{3+}, Cl^-, Br^-, SO_4^{2-}, and PO_4^{3-} left to right.

The fluorescence quenching data of the PL peak at 681 nm followed the Stern-Volmer equation by a static mechanism [35]:

$$F_0 / F - 1 = K_{sv} c \quad (1)$$

Where K_{sv} is the Stern-Volmer quenching constant, c is the analyte (NO_2^-) concentration, and F_0 and F are PL intensities of Pp-RhB dots at 681 nm in the absence and presence of NO_2^-, respectively. The Stern-Volmer plot shown in Fig. 3d was fitted by a linear Stern-Volmer equation over concentrations ranging from 5×10^{-10} to 2×10^{-9} M. The correlation coefficients (r^2) and K_{sv} were 0.9981 and 8.16×10^{-4} when determining NO_2^- over the linear concentration range of 2×10^{-11} to 2×10^{-9} M, respectively. The detection limit was estimated to be 1×10^{-11} M at a signal-to-noise ratio of 3. This detection limit was remarkable and satisfied the sensitivity requirement of NO_2^- detection for drinking water (7×10^{-5} M) defined by the US Environmental Protection Agency (EPA) and was much higher than the detection limit of other methods (Table. 1). [36-50]

The selectivity and specificity of these Pp-RhB dots are shown in Fig. 3g: Pp-RhB dots did not bestow any observable quenching effect upon many ions such as: Na^+, K^+, Li^+, Mg^{2+}, Zn^{2+}, Ni^{2+}, Cd^{2+}, Pb^{2+}, Fe^{2+}, Fe^{3+}, Al^{3+}, Cl^-, Br^-, SO_4^{2-}, and PO_4^{3-} with and without the presence of NO_2^-. This indicated that the Pp-RhB dots had excellent selectivity and specificity for NO_2^-. Further interfere experimental results (Fig. S6-9) also show the excellent selectivity and specificity for NO_2^- upon 45 kinds of disturbing substances. Moreover, the Pp-RhB dots show good stability when the pH is 4-10 (Fig. S10). This indicates the Pp-RhB dots can be used in most biotic environment.

The behaviour mechanism underpinning this fluorescent probe has been proposed and validated by fluorescent lifetime measurement experiments and its N1s spectra. As shown in Fig. 4a, the fluorescence of Pp-RhB dots was quenched as a result of a PET process arising from the amide bond in the Pp-RhB dots between its modulator (poly(o-phenylenediamine)) and RhB. Moreover, the enol form of Pp-RhB dots had a larger conjugation system than RhB which resulted in a red-shift of the PL spectra. However, when NO_2^- was added, the resulting C-N-NO bonding model prevented this PET, which enhanced the fluorescence emission. Meanwhile, the C-N-NO bonding model weakened the conjugation effects between poly(o-phenylenediamine) and RhB which resulted in a blue-shift of the PL spectra.

Fluorescent lifetime measurement experiments on Pp-RhB dots with different concentrations of NO_2^- were carried out in the search for further evidence supporting the quenching mechanism of the PL peak at 599 nm (Fig. 4b). The value of τ did not change ($\tau_0/\tau = 1$) for the molecules in static quenching where τ_0 and τ are the fluorescent lifetimes in the absence and presence of quencher (NO_2^-), respectively. This did not make any complex with the quencher, in its ground state, retain its original lifetime (τ_0). [51-53]

On the other hand, in dynamic quenching, $F_0/F = \tau_0/\tau$, and the lifetime decreased upon the addition of quencher. The lifetime of Pp-RhB dots did not change ($\tau \approx 4$ ns) upon NO_2^- addition which suggested that the quenching behaviour was due to the static quenching process over concentrations from 5×10^{-10} to 2×10^{-9} M. [30, 54-55] The N1s spectra (Fig. 4c) of the reaction products of Pp-RhB dots and $NaNO_2$ were used to explore the mechanism of the change in PL properties after the addition of NO_2^-. The N1s XPS spectrum indicated the existence of N-NO (399.1 eV) and $[Ph=N-(Et)_2]Cl^-$ (402.1 eV) bonding models in Pp-RhB dots.

The TOF-MASS spectrum was used to confirm the working mechanism of this sensing system. As shown in Fig. 4d, the peaks (black curve) located at m/z = 635.57, 737.86, 840.57, 941.96, 1045.11, 1146.57, 1249.39, 1351.47 and 1452.21 can be attributed to the amide compounds of RhB and the oligomers of oPD in Pp-RhB dots (the corresponding molecular structures of these amide compounds are shown in Fig. S11). However, when the NO_2^- was added, the TOF-MASS spectrum of Pp-RhB dots shows obviously change. Peaks (red curve) located at m/z = 664.77, 766.63, 869.80, 970.01, 1074.79, 1174.60, 1278.77, 1380.95, and 1481.33 can be attributed to the diazotized Pp-RhB dots (the corresponding molecular structures of these amide compounds are shown in Fig. S12). It is clear that, the m/z increased which is corresponding with the N-NO bonding mode of Pp-RhB dots after the NO_2^- added. This result is matched with the results of XPS and FTIR spectra.

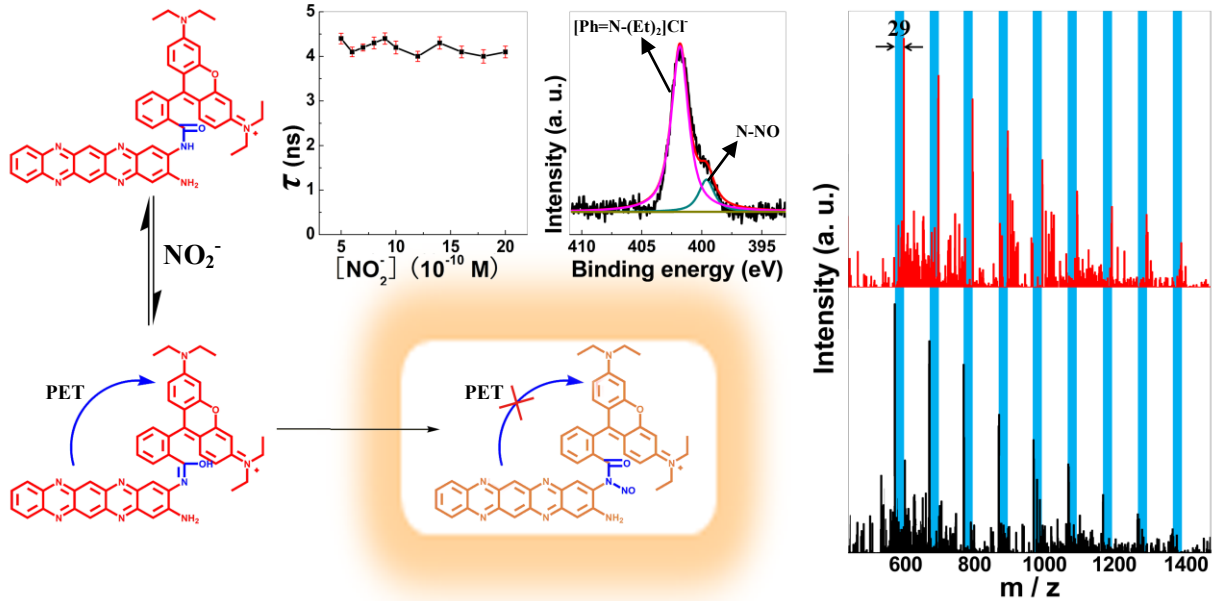

Fig. 4 (a) A schematic of the structure of Pp-RhB dots in the absence and presence of NO_2^- and the working mechanism of this fluorescence probe. (b) The lifetime of Pp-RhB dots plotted against the concentration of NO_2^-, where τ_0 and τ are the fluorescent lifetimes in the absence and presence of NO_2^-, respectively. (c) N1s spectra of the reaction products of Pp-RhB dots and $NaNO_2$. (d) MALDI-TOF-MASS spectrum for Pp-RhB dots (red curve) and the product of the reaction between Pp-RhB and $NaNO_2$.

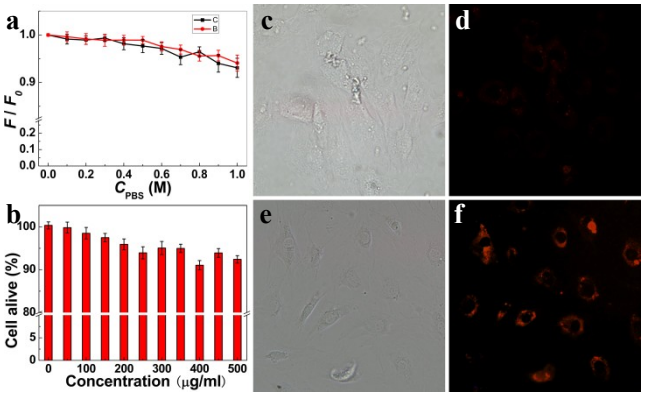

Fig. 5(a) Effect of ionic strength (PBS, pH = 5.6) on the PL intensity of Pp-RhB dots with (black curve) and without (red curve) the presence of NO_2^- at room temperature. F and F_0 are the PL intensities of Pp-RhB dots with and without the presence of PBS, respectively. The concentration of Pp-RhB dots was 1.0 mg/L, the concentration of NO_2^- was 0.1 mM. (b) Metabolic activity of HeLa cells treated with different concentrations of Pp-RhB dots. (c-f) HeLa cells loaded with 1 mL, 250.0 mg mL^{-1} Pp-RhB dots for 10 min. (c) Bright-field image of Pp-RhB dot-loaded cells, (d) Corresponding confocal fluorescence micrograph of (c). (e) Bright-field image of Pp-RhB dot-loaded cells treated with 0.5 μM $NaNO_2$ for 15 min. (f) Corresponding confocal fluorescence micrograph of (e).

For a practical bio-imaging application, the anti-jamming performance of Pp-RhB dots was important. Fig. 5a shows the PL stability of Pp-RhB dots against the ionic strength. There was no obvious change in PL intensity even with a concentrated phosphate buffer solution (PBS, pH = 6.8, which is the most commonly used buffer system in organisms) to 1.0 M. To assess the prospects of the Pp-RhB dots as a bio-imaging material, the HeLa cell line was used to evaluate the cytotoxicity of Pp-RhB dots. The activity of HeLa cells, treated with different concentrations of Pp-RhB dots (Fig. 5b), was observed. Different

concentrations of Pp-RhB dots (up to 500 μg/mL) were added to the cells cultured in 96 well-plates and incubated for 24 h. Subsequently, a standard assay was performed to assess the cell viabilities after Pp-RhB dot treatments. No significant reduction in cell viability was observed for cells treated with Pp-RhB dots even at concentrations of Pp-RhB dots of up to 500 μg/mL. These results indicated that Pp-RhB dots could be used for intracellular imaging.

The Pp-RhB dots were introduced into the HeLa cells to show their bioimaging capabilities using confocal microscopy. As shown in Fig. 5c and d, weak red luminescence was observed inside the cells, indicating that the Pp-RhB dots had been internalised by the HeLa cells and were mainly localised in the cytoplasm region. However, bright orange luminescence was observed inside the cells (Fig. 5e and f) after Pp-RhB dots loaded HeLa cells were treated with 0.2 μM $NaNO_2$ for 15 min. This result confirmed that Pp-RhB dots were capable of sensing NO_2^- through fluorescence responses in living cells.

Conclusions

In summary, we demonstrate a new semiconducting polymer dot, the Pp-RhB dots, which emit in the red wavelength range and can be used as an ultrasensitive fluorescence probe for NO_2^- *in vivo*. The fluorescence of Pp-RhB dots is decreased (φ = 0.014) as a result of fast photoinduced electron transfer (PET) between poly(o-phenylenediamine) and RhB, but the N-NO_2 bonding mode prevents PET progress, causing the fluorescence emission to be enhanced (φ = 0.92). The detection limit (2.0×10^{-11} M) is remarkable and is much higher than the detection limits of other methods. This work will be helpful for synthesising new bio-imaging materials with high anti-jamming performance, good stability, good biocompatibility, and high quantum yield.

Acknowledgement

This work was supported by China West Normal University Fund (12B017), Major Project of Education Department in Sichan (14ZA0125), National Natural Science Foundation of China (Grant no. 11104303) and the Chinese Academy of Sciences (Grant no. KGZD-EW-303 and XDA02040000).

Notes and references

[a] Chemical Synthesis and Pollution Control Key Laboratory of Sichuan Province, College of Chemistry and Chemical Engineering, China West Normal University, Nanchong 637002, China.
E-mail: liaozhang2003@163.com
[b] State Key Laboratory of Functional Materials for Informatics, Shanghai Institute of Microsystem and Information Technology, Chinese Academy of Science, Shanghai, 200500, China.
E-mails: yangsiwei@mail.sim.ac.cn and *gqding@mail.sim.ac.cn*
[c] Key Laboratory of Soft Chemistry and Functional Materials, Nanjing University of Science and Technology, Ministry of Education, Nanjing 210094, China
[‡] *These authors are co-first authors*
† Electronic Supplementary Information (ESI) available: [details of XPS survey, C 1s, O1s spectra, FTIR spectrum, and PL properties of Pp-RhB dots]. See DOI: 10.1039/b000000x/
**Corresponding author:*
Prof. Liao Fang, liaozhang2003@163.com
Dr. Siwei Yang, yangsiwei@mail.sim.ac.cn
Prof. Guqiao Ding, gqding@mail.sim.ac.cn

1 Y.-H. Chan, F. Ye, M. E. Gallina, X. Zhang, Y. Jin, I.-C. Wu, D. T. Chiu, *J. Am. Chem. Soc.*, 2012, **134**, 7309.
2 F. Ye, C. Wu, Y. Jin, M. Wang, Y.-H. Chan, J. Yu, W. Sun, S. Hayden, D. T. Chiu, *Chem. Commun.*, 2012, **48**, 1778.
3 P.-J. Wu, S.-Y. Kuo, Y.-C. Huang, C.-P. Chen, Y.-H. Chan, *Anal. Chem.*, 2014, **86**, 4831.
4 (a) C. Wu, S. J. Hansen, Q. Hou, J. Yu, M. Zeigler, Y. Jin, D. R. Burnham, J. D. McNeill, J. M. Olson, D. T. Chiu, *Angew. Chem. Int. Ed.*, 2011, **50**, 3430; (b) X.-G. Li, M.-R. Huang, Y. Yang, *Polymer*, 2001, **42**, 4099.
5 C. Wu and J. McNeill, *Langmuir*, 2008, 24, 5855.
6 (a) C. Wu, C. Szymanski, Z. Cain and J. McNeill, *J. Am. Chem. Soc.*, 2007, **129**, 12904; (b) M.-R. Huang, X.-G. Li, Y. Yang, *Polymer Degradation and Stability*, 2001, **71**, 31.
7 K. Y. Pu, K. Li, J. B. Shi and B. Liu, *Chem. Mater.*, 2009, **21**, 3816.
8 (a) C. Wu, H. Peng, Y. Jiang and J. McNeill, *J. Phys. Chem. B*, 2006, **110**, 14148; (b) X.-G. Li, M.-R. Huang, W. Duan, Y. -L. Yang, *Chem. Rev.*, 2002, **102**, 2925; (c) X.-G. Li, H.-Y. Wang, M.-R. Huang, *Macromolecules*, 2007, **40**, 1489.
9 (a) L. Zhou, J. Geng, B. Liu, *Part. Part. Syst. Charact.*, 2013, **30**, 1086; (b) X.-G. Li, X.-L. Ma, J. Sun, M.-R. Huang, *Langmuir*, 2009, **25**, 1675.
10 M. Bacon, S. J. Bradley, T. Nann, *Part. Part. Syst. Charact.*, 2014, **31**, 415
11 Y. Dai, H. Long, X. Wang, Y. Wang, Q. Gu, W. Jiang, Y. Wang, C. Li, T. H. Zeng, Y. Sun, J. Zeng, *Part. Part. Syst. Charact.*, 2014, **31**, 597.
12 R. Gokhale, P. Singh, *Part. Part. Syst. Charact.*, 2014, **31**, 433.
13 L. Tang, R. Ji, X. Li, K. S. Teng, S. P. Lau, *Part. Part. Syst. Charact.*, 2013, **30**, 523.
14 L. Fan, M. Zhu, X. Lee. R. Zhang, K. Wang, J. Wei, M. Zhong, D. Wu, H. Zhu, *Part. Part. Syst. Charact.*, 2013, **30**, 764.
15 Y. Dai, H. Long, X. Wang, Y. Wang, Q. Gu, W. Jiang, Y. Wang, C. Li, T. H. Zeng, Y. Sun, J. Zeng, *Part. Part. Syst. Charact.*, 2014, **31**, 509.
16 J. Sun, S. Yang, Z. Wang, H. Shen, T. Xu, L. Sun, H. Li, W. Chen, X. Jiang, G. Ding, Z. Kang, X. Xie, M. Jiang, *Part. Part. Syst. Charact.*, DOI: 10.1002/ppsc.201400189.
17 B.-J. de Gans, U. S. Schubert, *Langmuir*, 2004, **20**, 7789.
18 S. Kim, C.-K. Lim, J. Na, Y.-D. Lee, K. Kim, K. Choi, J. F. Leary, I. C. Kwona, *Chem. Commun.*, 2010, **46**, 1617.
19 C. Wu, B. Bull, C. Szymanski, K. Christensen and J. McNeill, *ACS Nano*, 2008, **2**, 2415.
20 W. Lijinsky, S. S. Epstein, *Nature*, 1970, **225**, 21.
21 I. A. Wolf, A. E. Wasserman, *Science*, 1972, **177**, 15.
22 C. Lina, V. S. Vasanthaa, K. Hoa, *Sensors and Actuators B*, 2009, **140**, 51.
23 L. Wang, B. Li, L. Zhang, L. Zhang, H. Zhao, *Sensors and Actuators B*, 2012, **171**, 946.
24 WHO, Guidelines for Drinking-Water Quality, 3rd ed., World Health Organization, Geneva, 2008.
25 F. Liao, S. Yang, X. Li, L. Yang, Z. Xie, C. Hu, L. He, X. Kang, X. Song, T. Ren, *Synth. Met.*, 2014, **189**, 135.
26 S. W. Yang, D. Liu, F. Liao, T. T. Guo, Z. P. Wu, T. T. Zhang, *Synth. Met.*, 2012, **162**, 2329.
27 F. Liao, S. Yang, X. Li, L. Yang, Z. Xie, C. Hu, S. Yan, T. Ren, Z. Liu, *Synth. Met.*, 2014, **189**, 126.
28 S.W. Yang, F. Liao, *Nano.*, 2011, **6**, 597.
29 S. W. Yang, F. Liao, *Synth. Met.*, 2012, **162**, 1343.
30 S. Yang, J. Sun, X. Li, W. Zhou, Z. Wang, P. He, G. Ding, X. Xie, Z. Kang, M. Jiang, *J. Mater. Chem. A*, 2014, **2**, 8660.
31 (a) X. Song, S. Yang, L. He, S. Yana, F. Liao, *RSC Adv.*, 2014, **4**, 49000; (b) P. He, J. Sun, S. Tian, S. Yang, S. Ding, G. Ding, X. Xie, M. Jiang, *Chem. Mater.*, 2015, DOI: org/10.1021/cm503782p. (c) T. Skaltsas, N. Karousis, S. Pispas, N. Tagmatarchis, *Nanotechnology*, 2014, **44**, 44540; (d) C. M. Jian, C. Gong, S. Q. Wang, S. F. Wang, X. M. Xie, Y. Wei, J. Y. Yuan, *European Polymer Journal*, 2014, **55**, 235.
32 S. Yang, C. Ye, X. Song, L. He, F. Liao, *RSC Adv.*, 2014, **4**, 54810.

33 F. Yu, P. Li, G. Li, G. Zhao, T. Chu, K. Han, *J. Am. Chem. Soc.*, 2011, **133**, 11030.
34 F. Yu, P. Li, B. Wang, K. Han, *J. Am. Chem. Soc.*, 2013, **135**, 7674.
35 S. Liu, J. Tian, L. Wang, Y. Zhang, X. Qin, Y. Luo, A. M. Asiri, A. O. Al-Youbi, X. Sun, *Adv. Mater.*, 2012, **24**, 2037.
36 R. Li, Z. Tao. Jiang, A. M. Lin, *Anal. Chem.*, 2011, **83**, 824.
37 Z. Lin, W. Xue, H. Chen, J. M. Lin, *Anal. Chem.*, 2011, **83**, 8245.
38 E. Pagliano, J. Meija, R. E. Sturgeon, Z. Mester, A. D'Ulivo, *Anal. Chem.*, 2012, 84, 2592.
39 V. Kumar, M. Banerjee nn, A. *Chatterjee Talanta*, 2012, **99**, 610.
40 P. Li, Y. Ding, A. Wang, L. Zhou, S. H. Wei, Y. M. Zhou, Y. W. Tang, Y. Chen, C. X. Cai, T. H. Lu, *ACS Appl. Mater. Interfaces*, 2013, **5**, 2255.
41 B. M. Jayawardane, S.Wei, I.D. McKelvie, S. D. Kolev, *Anal. Chem.*, 2014, **86**, 7274.
42 Y. L. Shao, P. C. You, F. Fang , H. L. Shu, J. N. Bing, G. Liu, C. T. Yang, Y. Xiong , Q. Y. Han, *Environ. Sci. Technol.*, 2008, **42**, 4467.
43 Y. H. Zhang, X. Y. Tian, Y. X. Guo, H. B. Li, A. J. Yu, Z. F. Deng, B. G. Sun, S. S. Zhang, *J. Agric. Food Chem.*, 2014, **62**, 3400.
44 X. X. Han, A. M. Schmidt, G. Marten, A. Fischer, I. M. Weidinger, P. Hildebrandt, *ACS Nano*, 2013, **7**, 3212.
45 A. D. Beaton, C. L. Cardwell, R. S. Thomas, V. J. Sieben, F. E. Legiret, E. M. Waugh, P. J. Statham, M. C. Mowlem, H. Morgan, *Environ. Sci. Technol.*, 2012, **46**, 9548.
46 H. Wu, S. H. Fan, X. Y. Jin, H. Zhang, H. Chen, Z. Dai, X. Y. Zou, *Anal. Chem.*, 2014, **86,** 6285.
47 W. L. Daniel, M. S. Han, J. S. Lee, C. A. Mirkin, *J. Am. Chem. Soc.*, 2009, **131**, 6362.
48 A. Ianoul, T. Coleman, S. A. Asher, *Anal. Chem.*, 2002, **74**, 1458.
49 B. Strehlitz, B. Gründig, W. Schumacher, P. M. H. Kroneck, K. D. Vorlop, H. Kotte, *Anal. Chem.*, 1996, **5**, 807.
50 N. Adarsh, M. Shanmugasundaram, D. Ramaiah, *Anal. Chem.*, 2013, **85**, 10008.
51 M. Rahman, H. J. Harmon, *Spectrochimica Acta Part A*, 2006, **65**, 901.
52 P. P. H. Cheng, D. Silvester, G. Wang, G. Kalyuzhny, A. Douglas, R. W. Murray, *J. Phys. Chem. B*, 2006, **110**, 4637.
53 F. Liao, S. Yang, X. Li, S. Yan, C. Hu, L. He, X. Kang, X. Song, T. Ren, *Synth. Met.*, 2014, **190**, 79.
54 P. K. Behera, T. Mukherjee, A. K. Mishr, *Journal of Luminescence*, 1995, **65**, 131.
55 S. Yan, S. Yang, L. He, C. Ye, X. Song, F. Liao, *Synth. Met.*, 2014, **198**, 142.